Total Charge-Transfer Cross Sections for He+ and Ar+ on K, Rb, and Cs: Near-Resonant Reactions Leading to Excited Final States*

J. R. Peterson and D. C. Lorents†
Stanford Research Institute, Menlo Park, California 94025
(Received 26 December 1968)

Total charge-transfer cross sections have been measured for He^+ and Ar^+ ions on K, Rb, and Cs atoms, using a crossed-beam arrangement. Ion-beam energies ranged from 10 to 1500 eV. The cross sections were all very large ($\gtrsim 50$ Å^2) for asymmetric reactions and give evidence of the anticipated importance of capture into excited states in near-resonant reactions. Predictions (for excited-state products) of a simple two-state theory provide qualitative agreement.

I. INTRODUCTION

We present here the results of a study of electron capture by the noble gas ions He^+ and Ar^+ in collisions with the alkali atoms Rb, Cs, and K. The measurements were undertaken[1] to examine the effect on the total electron-capture cross section, σ_{10}, of a near energy resonance (i.e., the change ΔE of the total electronic energy in the system is very small) when the initial reactants are in their ground states but one of the products is excited. Because the ionization potentials of alkali atoms are often very close to those of rare-gas atoms in their first excited states, ΔE is very large for reactions leading to ground-state products and quite small for certain excited final states (see Table I). One would expect such a condition to result in large cross sections even at fairly low relative velocities.

The importance of small values of ΔE in enhancing excitation in charge transfer had been discussed by Lindholm[2] and used by Dehmelt and Major,[3] but no cross-section measurements had been made when our work was initiated. While our measurements were in progress, Donnally *et al.*[4] reported rather large cross sections for the reaction $H^+ + Cs \rightarrow H(2s) + Cs^+ - 0.49$ eV. Several other studies have been made more recently. The work reported here was concerned only with total charge-transfer cross sections and did not specifically detect excitation.[5,6] None of the cross sections has an energy dependence characteristic of exact resonance, but their magnitudes are all much larger than one would expect for ground-state transitions ($\Delta E > 10$ eV). It can therefore be concluded that essentially all of the measured reactions lead to excited products (some of which are metastable).

II. DESCRIPTION OF THE EXPERIMENT

The crossed-beam arrangement shown in Fig. 1 was used for the measurements. An ion beam of variable energy passed perpendicularly through a

TABLE I. Energy defects for various neutral-atom final states (final ion in ground state).

$He^+(1s)$	ΔE(K)	ΔE(Rb)	ΔE(Cs)
$^1S_0$	20.22	20.39	20.67
2^3S	0.42	0.59	0.89
2^1S	−0.37	−0.20	0.08
2^3P	−0.62	−0.55	−0.27
2^1P	−0.97	−0.80	−0.52
3^3S	−2.48	−2.31	−2.23

	ΔE(K)		ΔE(Rb)		ΔE(Cs)	
Ar^+	$^2P_{3/2}$	$^2P_{1/2}$	$^2P_{3/2}$	$^2P_{1/2}$	$^2P_{3/2}$	$^2P_{1/2}$
$^1S_0$	11.42	11.60	11.59	11.77	11.87	12.05
$4s[\frac{3}{2}]_2^0$	−0.13	0.05	0.04	0.22	0.32	0.50
$4s[\frac{3}{2}]_1^0$	−0.20	−0.02	−0.03	0.15	0.25	0.43
$4s'[\frac{1}{2}]_0^0$	−0.30	−0.12	−0.14	0.04	0.15	0.33
$4s'[\frac{1}{2}]_1^0$	−0.40	−0.22	−0.23	−0.05	0.05	0.23
$4p[\frac{1}{2}]_1$	−1.49	−1.31	−1.32	−1.14	−1.04	−0.86

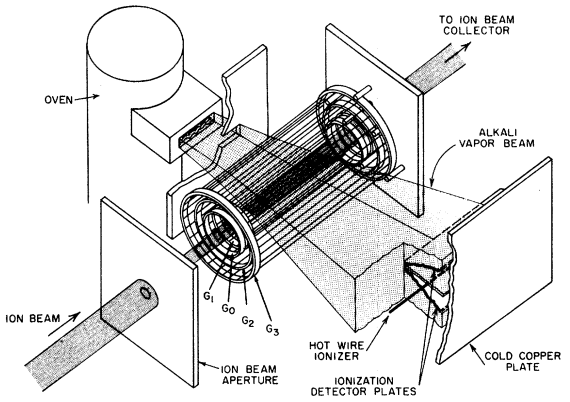

FIG. 1. Configuration of the beam interaction region. Most structural components have been omitted to simplify the figure. The oven can be moved vertically to stop the thermal beam.

thermal beam of alkali vapor. The slow ions produced in the intersection region were trapped in an electric potential trough and were collected on the inner of three concentric cylindrical grids placed coaxially with the ion beam. The ion beam was collected and measured after it left the slow ion trap. The vapor beam passed through the transparent grid structure and was condensed on a copper plate cooled to about – 5°C. Its flux density was monitored by a hot-wire ionizer in front of the condensing plate.

The slow ion current i_G is related to the ion-beam current i_T: for $i_G \ll i_T$,

$$i_G = i_T Q \int \rho dx \,, \tag{1}$$

where Q is the reaction cross section and ρ the alkali atom density at point x along the ion-beam path; it is assumed that ρ is constant over any cross sectional slice of the ion beam but may vary with x. These conditions were satisfied in the experiment. The effective limits of integration correspond, of course, to the boundaries of the vapor beam. To determine Q, we measured i_G, i_T, and the monitor current i_J'; $\int \rho dx$ was determined from i_J' by a method described below.

A. The Apparatus

1. *Vacuum Chamber*

There were two vacuum sections, each pumped by a 6-in oil diffusion pump trapped by a refrigerated baffle. One section contained the ion source and beam focusing electrodes; the other contained the alkali vapor oven and other apparatus associated with the beam interaction region. The two sections were connected by a cylindrical channel (2.5-cm long × 0.5-cm in diameter), which permitted the ion beam to pass but impeded the gas flow from the ion source section (at 10^{-4} Torr) to the measurement chamber (at about 1.5×10^{-6} Torr). The base pressure in the chamber was about 3×10^{-7} Torr.

2. *Ion Source and Beam Characteristics*

The ion source was of the electron-bombardment type[7] and produced very quiet beams of ions down to about 10 or 15 eV. Retarding-potential curves were taken to obtain the energy spread in the beams; an example for Ar^+ at 20-eV "nominal" energy (based on the ion-source grid potential) is presented in Fig. 2. The differentiated curve shows the beam to have a distribution peaked at 15.5 eV with a spread (full width at half-maximum) of 1.5 eV. A similar curve for He^+ peaked at 16 eV and had a spread of 3.2 eV. The actual energy spreads were probably smaller than these data suggest, but in any case they had no effect on the accuracy of the measurements. The beam energy characteristics varied slightly with source conditions but were generally constant during a single run. The difference between the most probable ion energy (15.5 eV in Fig. 2) and the nominal energy was determined whenever measurements were made below 50 eV. The resulting correction to the beam energy was most important for the lower energies, but it was also applied at the higher accelerating voltages.

The ion beam was focused by a three-element lens in the source chamber. The beam was defined in direction and cross-sectional area by the 0.51-cm-diameter channel between the two vacuum chambers and by a second aperture, also 0.51 cm in diameter, located about 10 cm downstream in

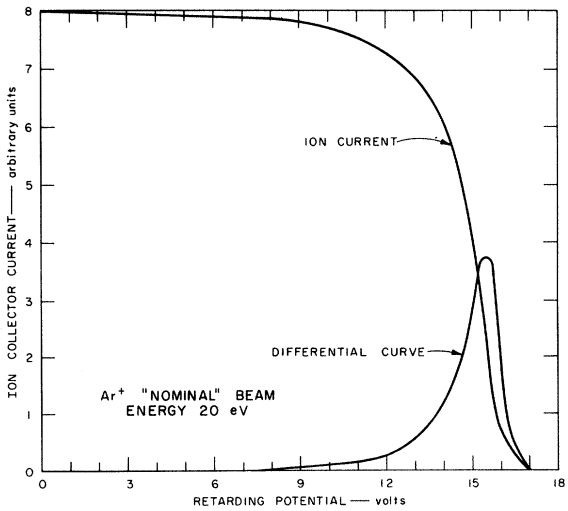

FIG. 2. Retarding-potential curve for Ar^+ beam.

front of the beam intersection region. The ion-beam currents, measured at the collector beyond the charge-transfer region, ranged from about $4\times10^{-9}A$ at 11 eV to $3\times10^{-6}A$ at 1 keV.

3. *Elements of the Interaction Chamber*

The essential components in this chamber were all housed in an aluminum box, which was cooled to about $-10°C$ during operation in order to trap stray alkali vapor. A thermally insulated 2.54-cm-diameter copper rod, which passed through the vacuum wall, conducted heat from the box to a dry-ice–acetone bath. Other cold surfaces mentioned below were cooled by thermal contact with the box.

a. *Vapor beam source.* The oven was a soft iron cylinder with a removable top, sealed with a 0.0025-cm nickel wire gasket. The exit orifice was rectangular in cross section and was filled with a "crinkle foil" thin-tube collimator to give a well directed vapor beam (see Fig. 1). The oven was heated by a molybdenum heater in the orifice wall to maintain high orifice temperatures for optimum beam collimation. It was loaded in a dry argon atmosphere and the alkali metal was covered with dry benzene until the chamber had been evacuated by a roughing pump.

The oven was mounted on a movable platform that could be raised or lowered mechanically from outside the chamber. For background measurements and during the oven warm-up periods, the oven was left in the down position; the beam was stopped by a cold copper plate located 1.27 cm in front of the orifice and about 0.64 cm from the outer grid of the ion trap. A rectangular aperture in this plate just at the ion-beam level defined the vapor beam when the oven was in the up position, as shown in Fig. 1.

b. *Slow ion trap.* Three concentric grids, G_1, G_2, and G_3 in Fig. 1, and two guard rings, G_0, at each end of G_1 were designed (a) to provide trapping fields for the slow ions, which were collected on G_1, and (b) to shield G_1 from stray, charged particle currents produced outside the beam intersection region. The incident ion beam was defined in cross section and angle by a 0.5-cm-diameter aperture before it entered the slow ion trap. The geometry was such that the beam could not hit G_1. The collimation was checked experimentally by using a smaller aperture (0.25 cm in diameter); no change in the measured cross sections resulted.

The cylindrical grids were made from 0.0038-cm tungsten wires stretched between thin nickel rings (2.54, 3.81, and 5.08 cm in diameter) at each end. The wires were held in tension by three stainless-steel screws on each ring, mounted on a Micalex plate at each end of the trap. The grid wires were spaced to provide high transparency (> 98% per grid) for both the vapor beam and photons generated in the beam interaction zone. During the design of the grid structure, the electric potential distributions were measured for different grid wire spacings and for several voltages on each grid. These distributions were used, along with the current-voltage curves made during the preliminary runs and actual measurements, to determine the proper operating potentials for the grids. For most ion-beam energies, the following potentials were used: $V_{G_0}=6$ to 10 V; $V_{G_1}=-3$ V; $V_{G_2}=22.5$ V; and $V_{G_3}=-12$ V. At ion energies below 50 eV, V_{G_0} was reduced somewhat to minimize defocusing of the ion beam. In all cases the potentials were set so that reasonable variations in them produced no change in the current to G_1.

c. *Vapor beam monitor.* A hot-wire surface ionization detector was used to monitor the alkali vapor flux. The tungsten wire and ion collector plates (stainless steel) were mounted immediately in front of the vapor beam condensing plate as indicated in Fig. 1. The ion collector plates formed a V-shaped collector, with a narrow slot aperture running the full length of the plates at the apex to pass a sample of the vapor in line with the ion-beam axis and the oven orifice. The wire, placed midway between the plates, was held in tension by a spring to keep it straight. The wire and the plates were long enough that a thin horizontal slab of the entire vapor target presented to the ion beam was monitored. The diameter of the tungsten wire was measured with an accurate micrometer. About 20 measurements taken over the length of the wire were used to determine the average diameter: $2.40\pm0.05\times10^{-3}$ cm.

In operation, the wire was kept a few volts negative with respect to the ground and the collector plates were at about -45 V. This arrangement assured complete collection of the ions by the plates.

The ion yield of the hot wire reached a saturation value when the wire heating current was raised to about 60 mA for Rb and Cs. The normal operating current was about 90 mA for these atoms. The yield saturated at about 80-90 mA for K, and a current of 100 mA was used during the experiment. Under these conditions the monitor yield was independent of changes in either the collector plate voltage or wire current, for all species, and we assume that 100% ionization and collection efficiencies obtained (see the discussion of errors below).

The monitor current i_J' obeys the relationship

$$i_J' = ew' v_m \int \rho' dx ,$$

where e is the electronic charge, w' the diameter

of the wire, v_m the mean speed of the vapor atoms in the oven[8,9] and ρ' the vapor density at the wire. $\int \rho' dx$ (at the monitor wire) is related to $\int \rho dx$ (at the ion-beam axis) by a geometric factor displaying the angular divergence of the vapor beam. A separate experiment was required to establish the factor

$$f = \int \rho dx / \int \rho' dx . \quad (2)$$

A second hot tungsten wire ionizer was streched between the ends of the ion trap along the position of the ion-beam axis, and its surface ionization current i_J was collected on G_1. A typical plot of the currents i_J and i_J' as a function of the vertical position of the oven is given in Fig. 3. Both currents are quite linear with oven position when the beam is partly cut off by the aperture, indicating a fairly uniform flux at the oven's orifice, but there is a slight (~ 2%) variation of both currents on the "flat" peak. The zero of the currents in Fig. 3 was taken as the background current with the oven down, well below the beam-defining aperture (at an indicator setting of about 7, to the left of the numbers on Fig. 3). A similar background subtraction procedure was used during the cross-section measurements. The ratio i_J/i_J' is also plotted in Fig. 3. It remains constant at 1.95 over the region when the oven is near the center of the defining aperture at a position indicator reading of 22.5. This value (1.95) of the ratio is uncorrected for the microammeter errors. The corrected ratio was close to 2.35 and increased less than 5% over a tenfold increase in vapor beam flux as the oven temperature was increased, reflecting a slow change in the vapor flow pattern with pressure. The ratio was found to be the same for Rb and Cs for the same oven vapor pressure as determined from vapor pressure-temperature curves. The value of f used in computing the cross section was taken from the experimental value for the oven temperature of each run.

The ratio

$$i_J/i_J' = w \int \rho dx / (w' \int \rho' dx) = f$$

since $w' = w$ by micrometer measurement. The atom target density $\int \rho dx$ in Eq. (1) was determined from the monitor current i_J' using the relation

$$\int \rho dx = i_J / e w v_m = f i_J' / e w' v_m . \quad (3)$$

B. Procedure

Relative measurements were taken in the following manner. With the aluminum box cooled, the oven was heated to the desired temperature

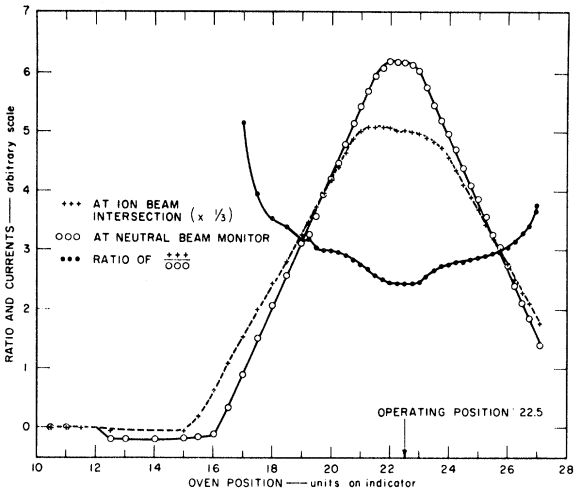

FIG. 3. Yields of vapor beam detectors versus oven position.

while in the down position. About an hour was required for all temperatures (measured by suitably placed thermocouples) and background currents to reach equilibrium values.

For each desired value of the ion-beam energy, several measurements were made, alternately with the oven lowered so that the vapor beam was cut off, and then with the oven raised. The differences Δi_{G_1} and $\Delta i_J'$ between the vapor beam "on" and "off" values, along with the incident ion-beam current i_T, yielded relative cross sections in the form $Q_{\text{rel}} = \Delta i_{G_1} (\Delta i_J' i_T)^{-1}$. The oven temperature was usually set to achieve vapor densities such that about 2% of the ion beam underwent charge transfer at 250 eV; that is, $\Delta i_{G_1} \approx 0.02\, i_T$, and i_T was correspondingly reduced by 2% when the oven was raised. Under these conditions Eq. (1) is valid and the slow ion yield is linear with $\Delta i_J'$ and Q. As the ion energy was changed, the validity of the current readings was tested. At higher energies the potentials on the ion collector suppressor grids and on the ion trap guard rings G_0 were rearranged to prevent positive ions emitted from the ion collector from reaching G_1 and to suppress the more energetic secondary electrons. At ion energies below 100 eV, these potentials were reduced appropriately to prevent distortion of the beam ion trajectories. In all cases, the relative cross section was independent of reasonable variations in any of the electrode potentials about their operating values. We also found that the slow ion yields were linear with the vapor density. Further, the cross sections were unaffected by a sixfold increase in the monitor current and were independent of the ion-beam current.

In addition to the charge-transfer ions, there also existed a slow ion current to G_1 caused by

photo-ionization of the vapor beam (by photons emanating from the ion source). The resulting slow ion background was essentially constant during a given run. This background became increasingly important toward lower ion-beam energies where both the ion-beam current and the charge-transfer cross sections decreased. At beam energies below 150 eV it was necessary to determine the contribution to i_{G_1} due only to charge transfer by taking measurements with the ion-beam off and on, with the alkali oven both up and down, and performing appropriate subtractions. The low energy limit of the measurements was reached when the charge-transfer ion current was reduced to a magnitude comparable to the photo-ionization background and the uncertainties in this double subtraction procedure (due mainly to beam instabilities) became unacceptable.

Collisional ionization of the vapor atoms by ion impact ($A^+ + B \rightarrow A^+ + B^+ + e$) can also yield slow ions. It was not possible in our apparatus to shield grid G_2 against electrons from other sources in order to measure the electrons produced by the ionization reactions. The negative current to G_2 always exceeded the slow ion current, even with the vapor beam off. This background was found to be associated with the ion beam and apparently due to secondary electrons from the aperture in front of the charge-transfer region. We were able to show that these electrons did not interfere with the slow ion measurements, but they did prevent the direct measurement of the current due to ion-impact ionization of the vapor atoms. Perel *et al.*[8] have reported that the total electron current from $Rb^+ + Rb$ collisions at 10 keV was less than 2% of the charge-transfer current. At an equivalent ion speed (1.5×10^7 cm/sec), the $He^+ + Rb$ ionization cross section is probably smaller than that of $Rb^+ + Rb$; thus it should be less than 2% of the electron-capture cross section. Although the ionization cross section for Cs may be somewhat larger, it is highly unlikely that any of the measured cross sections were increased by more than 5% due to this background. This effect is included in the total error estimated below.

C. Calculation of the Cross Sections

The total charge-transfer cross sections were obtained from the equation

$$Q = (ew'v_m/f)(\Delta i_{G_1}/i_T \Delta i'_J), \qquad (4)$$

which follows from Eqs. (1) and (3) with i_G and i'_J replaced by Δi_G and Δi_J, the changes in these currents caused by raising the vapor oven. Again, the quantity

$$\Delta i_{G_1}/i_T \Delta i'_J$$

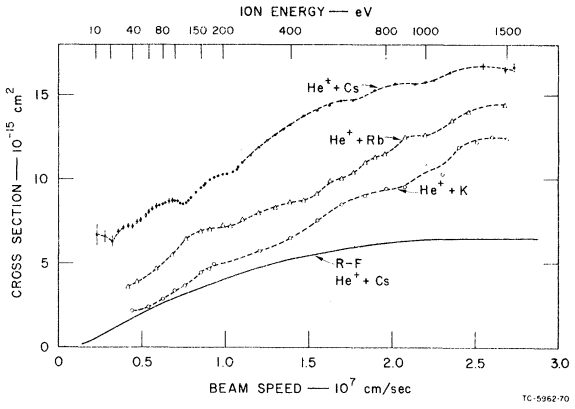

FIG. 4. Total charge-transfer cross sections for He^+ in K, Rb, and Cs. Error bars indicate random statistical errors for $He^+ + Cs$ results. Solid line is Rapp-Francis prediction for $He^+ + Cs$.

is the relative cross section described above, e is the electron charge, w' is the diameter of the hot wire of the vapor beam monitor, f is the monitor constant defined by Eq. (2), and the mean speed of the oven vapor [8,9]

$$v_m = \left(\frac{8kT}{\pi M}\right)^{\frac{1}{2}} = 1.46\times10^4\left(\frac{T}{M}\right)^{\frac{1}{2}} \text{ cm/sec},$$

where T is the oven temperature (°K) and M is the mass of the vapor atom (amu).

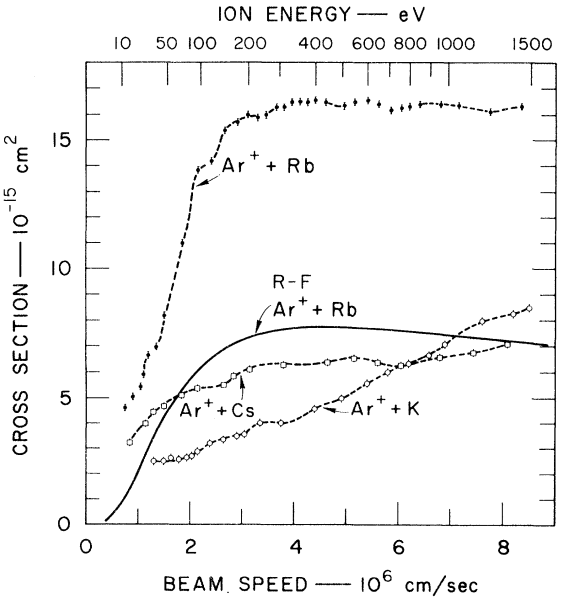

FIG. 5. Total charge-transfer cross sections for Ar^+ in K, Rb, and Cs. Error bars indicate random errors. Rapp-Francis calculation for $Ar^+ + Rb$ is given by solid curve.

D. Results

The cross sections for He^+ and Ar^+ were measured over the ion energy range from 10 to 1500 eV in the vapors of Rb and Cs and from 35 to 1500 eV in K. The results are presented in Figs. 4 and 5 and in Table II. The $He^+ + Cs$ reaction cross section was studied the most thoroughly, and some of the data points taken at small energy intervals are not included in Table II.

TABLE II. Charge-transfer cross sections (10^{-14} cm^2) for He and Ar ions at various energies (eV) and speeds (10^7 cm/sec) in K, Rb, and Cs vapors.

	He^+				Ar^+			
Lab energy	Speed	Q(K)	Q(Rb)	Q(Cs)	Speed	Q(K)	Q(Rb)	Q(Cs)
11	0.230			0.67 ±.06	0.073		0.46 ±.02	
16	0.28			0.66 ±.03	0.088		0.505 ±.02	0.320
21	0.32			0.63 ±.03	0.101		0.545 ±.01	
26	0.36			0.69 ±.01	0.112		0.595 ±.01	0.400
31	0.39			0.715 ±.01	0.122		0.665 ±.007	
36	0.42		0.36	0.723 ±.01	0.132		0.700	0.445
40	0.45	0.215		0.720	0.40	0.247		
46	0.47		0.39	0.750	0.149		0.820	0.463
50	0.49			0.760	0.155	0.244		
60	0.54	0.237		0.810	0.170	0.248		
71	0.59		0.47	0.840	0.185	0.254	1.100	0.510
80	0.62	0.286		0.853	0.196	0.261		
90	0.66			0.870	0.208	0.264		
96	0.68		0.55	0.876	0.215		1.385	0.540
100	0.70	0.337		0.872	0.220	0.285		
105	0.71			0.870				
110	0.73			0.860				
115	0.75			0.858				
121	0.77		0.645	0.860	0.242	0.365	1.425	
125	0.78	0.318		0.875				
130	0.79			0.893				
140	0.82			0.923				
146					0.266		1.540	0.552
150	0.85	0.335	0.690	0.950	0.269	0.441		
170	0.91	0.462	0.700	0.998	0.287	0.344	1.570	0.582
190	0.96			1.020				
200	0.98	0.498	0.725	1.030	0.311	0.353	1.600	0.610
225	1.03		0.72	1.035	0.330		1.590	
230	1.05			1.050				
240	1.08			1.070	0.342	0.401		
250	1.10		0.760	1.100	0.348		1.600	
275	1.15			1.170	0.365		1.630	
300	1.200		0.800	1.190	0.381	0.400	1.630	0.630
325	1.25	0.572		1.230	0.396		1.650	
350	1.30		0.832	1.265	0.411		1.650	
375	1.35			1.30	0.426		1.650	
400	1.39	0.651	0.865	1.325	0.440	0.458	1.655	
450	1.47		0.875	1.380	0.466		1.650	0.645
500	1.55	0.755	0.915	1.410	0.492	0.498	1.635	
550	1.63		0.990	1.445	0.516		1.650	0.655
600	1.70	0.850	1.005	1.470	0.539	0.555	1.655	
650	1.77		1.040	1.470	0.561		1.640	0.640
700	1.84	0.899	1.100		0.582	0.598	1.620	
750	1.90		1.130	1.530	0.602		1.630	0.630
800	1.96	0.948	1.150		0.622	0.632	1.630	
850	2.02			1.570	0.641		1.640	
900	2.08		1.250		0.660	0.674		
950	2.14			1.570	0.678		1.640	0.660

TABLE II. *Continued.*

	He^+				Ar^+			
Lab energy	Speed	Q(K)	Q(Rb)	Q(Cs)	Speed	Q(K)	Q(Rb)	Q(Cs)
1000	2.20	1.09	1.265	1.580	0.695	0.710		
1050	2.25			1.590	0.713		1.640	
1100	2.31	1.03						
1150	2.36		1.350	1.640	0.745			0.680
1200	2.42	1.19			0.761	0.798		
1250	2.46		1.400		0.778		1.610	
1300	2.52	1.22						
1350	2.55			1.680	0.808			0.710
1400	2.61	1.25			0.821	0.829		
1450					0.837		1.630	
1495	2.68	1.24	1.445	1.655	0.850	0.855		
1550	2.73			1.67				

A few errors are indicated for low energy points. These are estimates of the experimental standard error. When errors are not quoted, the random error is about 1% for $He^+ + Cs$ below 900 eV and 2% above, and about 3% for the other reaction cross sections above 100 eV. The assumption of 100% surface ionization efficiency for the hot wire alkali beam flux detector is undoubtedly realistic for the Rb and Cs beams; however, it may be an overestimate for the K beams. Datz and Taylor[10] found a maximum efficiency of 86% for a clean W wire, while an oxide coating on the wire can yield 100%. No attempts were made to clean our wire, beyond washing it with distilled water; thus it was probably initially oxide coated. Although we did not observe any change in efficiency (or in the cross sections obtained on different days), the results may nevertheless be as much as 15% too high because of the 100% efficiency assumption. The total error is estimated to be less than 10% for the reactions involving Rb and Cs, and 20% for the K results.

III. DISCUSSION

The noteworthy characteristics of the cross sections shown in Figs. 4 and 5 are the magnitudes, the general velocity dependence, and the structure (which is particularly evident in the $He^+ + Cs$ reaction).

The magnitudes are larger than 0.5×10^{-14} cm^2 except at the lowest energies, and exceed 1.5×10^{-14} cm^2 at the maxima. Cross sections of this magnitude can only result from near-resonant reactions when the transition can occur with high probability at large internuclear separations. For instance, the Stueckelberg two-state theory[11] estimates a maximum total cross section of about πR_x^2 when R_x is the internuclear distance at the crossing of the potential-energy curves of the initial and final molecular states (use of a random-phase approximation gives $\sim \frac{1}{2}\pi R_x^2$ for Stueckelberg's treatment). For the magnitudes of Q_{max} here we find R_x occurs at at least 7 Å. Because the forces between the atoms are small at these distances, such crossings can occur only between states whose internal energies do not lie far apart at infinite nuclear separations, that is, between states satisfying the criterion for near-resonant reactions. For these reactants it can be deduced that nearly all reactions proceed directly to excited states of one of the products. In the reactions involving He^+ ions studied here, near-resonant reactions can yield either excited He atoms or excited alkali ions. However, excitation of the final ion involves at least one closed-shell electron of the ion and perhaps the valence electron as well. At these comparatively low energies such events are probably less frequent than the electron transfer producing excited He atoms, which need only be an outer electron process. For Ar^+, near-resonant conditions occur only when the electron capture yields excited Ar atoms. The relative populations of the various probable final states of these reactions have not yet been measured for these reactions, but the resulting excited neutral beams have been used to produce He^- beams,[12,13] and to measure de-excitation cross sections.[14]

Although the cross sections are large, the energy dependences are not characteristic of exact, or "accidental," resonance which generally follows the relationship $Q^{1/2} = a - b\ \ln E$. Since there have been no detailed theoretical treatments of these reactions, it is not possible to offer any other than qualitative arguments for the energy dependence. We note, however, that it is under conditions satisfied by the reactions studied here that the Rapp-Francis (RF) approximation[15] is at its best, i.e., when the ionization potentials of the atoms are small (here the final rare-gas atom is considered to be in an excited state) and the interaction occurs at large internuclear distances. For this reason we were prompted to compare

the predictions of the RF theory with some of the experimental results. Lee and Hasted[16] have presented the RF approximation in a useful form by making some additional simplifications that are consistent with the restrictions already imposed by Rapp and Francis. This formulation was used to compute the cross sections for $He^+ + Cs$ and $Ar^+ + Rb$.

The calculation involves the mean ionization potential of the two atoms and the energy defect ΔE, plus a statistical weighting factor. The computations thus required some assumptions about the initial and final atomic states, as well as the statistical weights of the reaction channels. For $He^+ + Cs$, the initial states are $He^+(1s\,^2S_{1/2})$ and $Cs(5p^6 1s\,^2S_{1/2})$. The final states were assumed to be $Cs^+(^1S_0)$ and only the four excited He states $(1s2s)\,^1S$, ^3S, and $(1s2p)\,^1P$, ^3P. The RF theory considers only two states, and the normalization procedure thus cannot apply to the cases treated here. We have considered each of four final states (characterized by the appropriate value of ΔE) to participate independently, weighted relatively by the statistical weights of their spin states, and then averaged the sum by dividing each weighting factor by two, since each pair of spin states was used for two cross sections. The total cross section Q_T was taken as a sum of the (independent) individual contributions; thus

$$Q_T = \tfrac{3}{4}[Q(^3S) + Q(^3P)] + \tfrac{1}{4}[Q(^1S) + Q(^1P)] .$$

The P-state cross sections receive no more statistical weight than the s-state cross sections because we assume that only Σ intermediate molecular states can arise from the two s orbitals of the initial valence electrons. The RF theory considers only transitions in which symmetry of the total (spinless) wave function is conserved. Another possible choice would have increased the results by a factor of 2 (the individual cross sections would be simply added). It is clear, on the other hand, that one cannot simply increase the denominator indefinitely as more states are considered, as this procedure will lead to steadily decreasing cross sections as states with larger ΔE's are added, whose cross sections are negligible. Our procedure is admittedly arbitrary, and a better theory would be desirable.

For $Ar^+ + Rb$, the Ar^+ beam was assumed to consist of $\frac{2}{3}$ $Ar^+(3p^5\ 2P_{3/2})$ and $\frac{1}{3}$ $Ar^+(3p^5\,^2P_{1/2})$. The final Ar atom was restricted to the near-resonant states $(P_{1/2})4sP_1$, $(P_{1/2})4sP_0$, $(P_{3/2})4s$ P_2, and $(P_{3/2})4sP_1$, where the symbols in the parentheses indicate the state of the ionic core. The multiplicative factor for each partial reaction cross section consisted of the statistical weight of the core state times the weight of the final atom as follows: the $P_{1/2}$ core (with the weight $\frac{1}{3}$) can produce P_1 and P_0 states with the weights $\frac{3}{4}$ and $\frac{1}{4}$, respectively; thus the cross sections for these states will contribute to the total as $\frac{1}{3}\times\frac{3}{4}$ $Q(P_1)$ and $\frac{1}{3}\times\frac{1}{4}$ $Q(P_0)$. Similarly, the states with the $(P_{3/2})$ can contribute according to $\frac{2}{3}\times\frac{5}{8}$ $Q(P_2)$ and $\frac{2}{3}\times\frac{3}{8}$ $Q(P_1)$.

The results are shown in Figs. 4 and 5 along with the experimental data. The calculated cross sections are less than half the size of the experimental ones, but the dependence on ion speed is quite similar except at the lowest values. Indeed if the $Ar^+ + Rb$ theoretical results are multiplied by 2.2, the experimental data are tracked remarkably well (to within 10%) above 20 eV. Similarly, an increase in the $He^+ + Cs$ theoretical results by a factor of 2.5 brings them within 10% of the experimental values for He^+ energies above 20 eV. The approximation of atomic orbitals by simple one-electron wave functions makes this theory generally predict low cross sections, and it is undoubtedly the special nature of the particular reactions studied here (which occur at large distances where perturbations of the electron core are small) which allows the theory to provide the qualitative agreement that it does.

Over the range of our measurements the experimental cross sections certainly do not have the $Q^{1/2} = a - b\ \ln v$ velocity dependence of the accidental resonance case. The general shapes of the cross-section curves are predicted fairly well by the Rapp-Francis theory as we have applied it, and in its light the fact that the cross sections do not show an exact-resonant behavior can be explained by the existence of several possible final states with different values of ΔE.

The total cross sections $He^+ + Cs$ have also been measured by Donnally and Thoeming[12] at 3 keV and by Schlachter *et al.*[13] for He^+ energies between 1.5 and 25 keV. Their results are shown, along with the present results and the RF predictions, on a plot of $Q^{1/2}$ versus $\ln v$ (v = ion speed

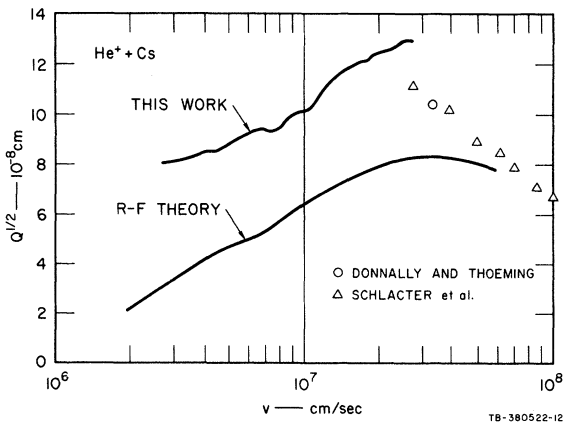

FIG. 6. $Q^{1/2}$ versus log$E$ plot of these and other experimental results for $He^+ + Cs$. Predictions of Rapp-Francis theory are also shown.

in cm/sec) in Fig. 6. Our results at 1450 eV are about 30% higher than those of Schlachter *et al.* at about 1500 eV, the only energy common to the measurements. This disagreement is not understood, but it probably originates in the calibration of the vapor target thickness (integrated vapor density along the ion-beam path). There is doubtless some error in each experiment.

Our absolute errors stem mainly from the measurements of the wire diameters of the two surface ionization detectors (5%), the current meter calibrations (2%), and the assumption that the vapor beam density was uniform over any particular cross section of the ion beam (probably < 5%; variations *along* the ion-beam path were accounted for). The greatest absolute uncertainties in the measurements of Schlachter *et al.* probably were connected with the calibration of their Cs gauge, which required a fit of the ionization detector yield (a relative measure of the efflux of Cs from a sampling orifice in the oven) to published values of Cs vapor pressure versus temperature. The vapor pressure of Cs is a very steep function of temperature, and a 30% variation occurs over a temperature change of less than 4°K in their range of operation. Their relative uncertainties were about 10%. Donnally and Thoeming's absolute values also depend on vapor pressure curves and oven temperature measurements. They estimate their error at +15%.

In any case, it appears that the value of the $He^+ + Cs$ cross section reaches a maximum at about 1500 eV, and that our highest energy corresponds to a maximum in the cross section, and the range covered by Schlachter *et al.* is in the high energy region, where $Q^{1/2} \sim a - b \ln E$. The RF theory is in rough agreement with this behavior (see Fig. 6).

When this work was originally undertaken, one of the reasons for expecting that near-resonant reactions would have high cross sections was that this was predicted by a simple application of Massey's adiabatic criterion.[17] Now that it has become clear that many inelastic processes with large energy separations at infinity have respectable cross sections even at very low energies, the naive form of the adiabatic criterion no longer appears justified, and it is being largely superseded by a return to the curve-crossing formalism. (There is a very close connection between the Landau-Zener curve-crossing theory and a more sophisticated view of the adiabatic criterion that is entirely consistent with Massey's original point of view.)[18] If we consider the molecular states formed when two atoms approach each other, it is clear that some of the crossings between them are much more likely to fall at large distances R_x if the energy separation ΔE between the states at infinity is small. Since the cross section in question is essentially πR_x^2 multiplied by a probability factor, the opportunity for a process having a large cross section is greatly enhanced if ΔE is small. A more quantitative argument also shows that the peak in the total cross section is likely to occur at lower energies as ΔE decreases. Thus the curve-crossing theory leads to results very similar to those of the Massey adiabatic criterion; it also allows for more quantitative predictions and a more detailed description.

Some structure, in the form of undulations in the curves drawn through the data points, is present in all cases studied. It is most evident in the $He^+ + Cs$ and $Ar^+ + Rb$ reactions which were examined most thoroughly. Such undulations have been observed in total cross sections of both symmetric and unsymmetric reactions between alkalis[8,19,20] and have been predicted theoretically.[21,22] The oscillations in the alkali ion-atom reaction cross sections are periodic when the cross sections are plotted against the reciprocal of the ion speed.

The theory of such oscillations was first developed for the symmetric situation, but Lichten pointed out that the same argument applies with only minor modification in the asymmetric case. Lichten's discussion[21] was focused primarily on oscillations in differential cross sections, but the fact that such oscillations at high energies are essentially independent of the scattering angle and are uniformly spaced in reciprocal speed means that the same behavior will appear in the corresponding total cross section. Thus the behavior seen by Perel *et al.* in the alkali ion-atom total cross sections[8] is really of the same origin as the oscillating behavior seen by Everhart *et al.* in rare-gas differential charge-exchange cross sections at high energies.

In the cases reported here more than one final

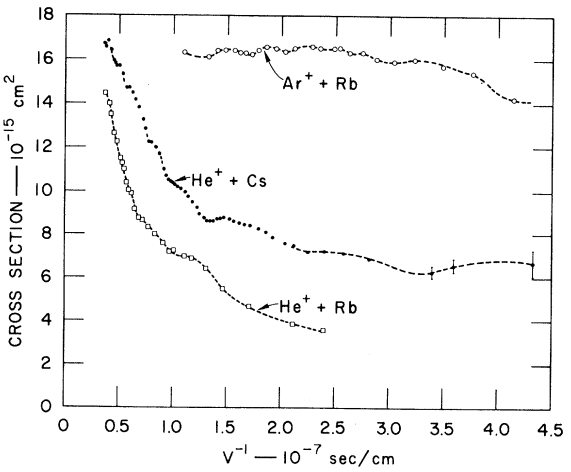

FIG. 7. Plot of three cross sections versus inverse beam speed.

state is involved in each cross section, so one can expect more complicated structures than occur in pure alkali or symmetric cases, and some of the patterns may be washed out by competing effects. For general interest, three of the better sets of data are plotted against reciprocal speed in Fig. 7 (note that the curves must approach the origin). Some oscillations are suggested, but no attempt has yet been made to analyze them in detail.

ACKNOWLEDGMENTS

We would like to acknowledge the generous assistance of George Conklin and Ralph Leon in fabricating and maintaining the equipment, and also many fruitful discussions with Dr. Felix T. Smith.

---

*Supported in part by the Advanced Research Projects Agency and monitored by the U.S. Army Research Office, Durham under Contract DA-31-124-ARO-D-220.

†Presently on leave of absence at University of Aarhus, Denmark.

[1]D. C. Lorents and J. R. Peterson, Fourth International Conference on the Physics and Electronics of Atomic Collisions, Quebec, Canada, 1965 (Science Bookcrafters, Hastings-on-Hudson, New York 1965), p. 328.

[2]E. Lindholm, "Recombination Energies of Positive Atomic and Molecular Ions," Abstracts of Papers of the Second International Conference on the Physics and Electronics of Atomic Collisions, Boulder, Colorado, 1961 (W. A. Benjamin, Inc., New York, 1961) p. 177.

[3]H. G. Dehmelt and F. G. Major, Phys. Rev. Letters 8, 213 (1962).

[4]B. L. Donnally, T. Clapp, W. Sawyer, and M. Schultz, Phys. Rev. Letters 12, 502 (1964).

[5]We have more recently measured cross sections for the production of optical excitation in some of these transfer reactions (see Ref. 6).

[6]A. Salop, D. C. Lorents, and J. R. Peterson, Bull. Am. Phys. Soc. 13, 204 (1968).

[7]D. C. Lorents and W. Aberth, Phys. Rev. 139, A1017 (1965).

[8]J. Perel, R. H. Vernon, and H. L. Daley, Phys. Rev. 138, A937 (1965).

[9]The need to use the average speed in the oven, rather than the average speed of beam atoms leaving the oven orifice may be deduced from arguments given by William J. Taylor, J. Chem. Phys. 38, 779 (1963).

[10]S. Datz and E. H. Taylor, J. Chem. Phys. 25, 389 (1956).

[11]See, for instance, N. F. Mott and H. S. W. Massey, The Theory of Atomic Collisions (Oxford University Press, New York 1965) 3rd ed. p. 651.

[12]B. L. Donnally and G. Thoeming, Phys. Rev. 159, 87 (1967).

[13]A. S. Schlachter, D. H. Lloyd, P. J. Bjorkholm, and L. W. Anderson, Phys. Rev. 174, 201 (1968).

[14]M. Hollstein, D. C. Lorents, and J. R. Peterson, Bull. Am. Phys. Soc. 13, 197 (1968).

[15]D. Rapp and W. E. Francis, Proc. Roy. Soc. (London) A268, 2349 (1964).

[16]A. R. Lee and J. B. Hasted, Proc. Roy. Soc. (London) 85, 673 (1965).

[17]H. S. W. Massey, Rept. Progr. Phys. 12, 248 (1949).

[18]F. T. Smith, in Proc. Eighth International Conference n Phenomena in Ionized Gases, Vienna, 1967 (International Atomic Energy Agency, Vienna, 1968) p. 75.

[19]J. Perel and A. Y. Yahiku, in Fifth International Conference on the Physics and Electronics of Atomic Collisions, Leningrad, 1967 (Leningrad Nauka Publishing House, Leningrad, 1967) p. 400.

[20]J. M. Peek, T. A. Green, and J. Perel, Phys. Rev. Letters 20, 1419 (1968).

[21]W. Lichten, Phys. Rev. 131, 229 (1963); 139, A27 (1965).

[22]F. J. Smith, Phys. Letters 20, 271 (1966).